14th International Symposium on Turbulence and Shear Flow Phenomena (TSFP14)
Heidelberg, Germany, July 28–31, 2026

FREE-STREAM TURBULENCE EFFECTS ON BLUFF BODIES' DRAG AND WAKES : FROM ACADEMIC TO REALISTIC DESIGNS

Pierre-Yves Passaggia
PRISME Laboratory
University of Orléans
8, Rue Léonard De Vinci
45072, Orléans, France
pierre-yves.passaggia@univ-orleans.fr

Ahmed Abed Meraim
PRISME Laboratory
University of Orléans
8, Rue Léonard De Vinci
45072, Orléans, France
ahmed.abed-meraim@univ-orleans.fr

Azeddine Kourta
PRISME Laboratory
University of Orléans
8, Rue Léonard De Vinci
45072, Orléans, France
azeddine.kourta@univ-orleans.fr

1 Introduction

Near wakes contribute for the most part to the total drag of bluff bodies. These turbulent wakes are strongly affected by free-stream conditions, which essentially, manifest under the effect of free-stream turbulence and side winds. Although academic vehicle configurations such as the Ahmed body have been studied under the effect of free-stream turbulence, its effect on models displaying realistic thus complex configurations is difficult to reach at the full scale and hardly reported in the literature. In addition, direct comparisons between the Ahmed body and a realistic car model have rarely been attempted (Bonnavion, 2018). In this paper, we analyse the effect of free-stream turbulence on the near wake and the resulting drag between an Ahmed body and a 2004 Citroën C4 coupé model. This hatchback model is representative of mid-range city vehicles that are widely popular in Europe.

Near-wake bluff body analyses begin with the definition of an interface used to project the mass and momentum equations to diagnose the exchanges of these fluxes between the wake and the outer flow. For example, Grandemange *et al.* (2013*a*) and Passaggia *et al.* (2021) used the dividing streamline, also known as the separatrix, to estimate the momentum budget in the mid vertical plane of the Ahmed body. They showed that, in the case of the Ahmed body, four quantities are relevant: the shear and normal Reynolds stresses, the mean pressure, and the curvature of the mean streamline. Passaggia *et al.* (2021) used the same approach on the same body subject to free-stream turbulence generated by bi-planar grids and showed that homogeneous and isotropic turbulence significantly modified the aerodynamic drag and its wake properties.

However, using the separatrix as an interface imposes two major constraints; (i) streamlines are only well suited for essentially two-dimensional flows which restricts the analysis to the mid vertical and horizontal plane and (ii) there is no net mass flux across a streamline, which prevents a possible mass-entrainment analysis. An alternative approach was proposed in Stella *et al.* (2017*a*) using the Recirculation Region Interface (RRI), which is defined along the zero-mean streamwise velocity. While the separatrix is located along the centre of the shear layers, the RRI crosses the centre of the vortices, thereby defining the region where mass entrainment and momentum are linked. Zeidan *et al.* (2023) carried out a similar analysis in the near-wake of a flat-back Ahmed body, whereas Khan *et al.* (2024) extended this approach to the analysis of the three-dimensional wake. In this paper, we apply the same analysis to the Ahmed body and the Citroën C4 model subject to turbulence.

In what follows, we analyse the near-wake characteristics alongside mass and momentum budgets in order to understand and diagnose base- and total-drag variations which depend non trivially on the turbulent intensity and the integral lengthscale in both cases. In particular, we show that while the mass entrainment budgets evolves similarly for both geometries, the momentum budget shows an opposite behaviour, highlighting some limits of the Ahmed body as a relevant surrogate to realistic car geometries.

2 Experimental setup

The full-scale square-back Ahmed body with dimensions $[L,W,H] = [1.044, 0.340, 0.288]$ m (Ahmed *et al.* (1984)) is compared against the results obtained from a Citroën C4 with similar dimensions $[1.074, 0.437, 0.352]$ m. Experiments were carried out in the S1 wind tunnel at PRISME laboratory (Orléans, France). The test section of this closed-loop wind tunnel is a 2×2 m^2 and extends over 5 m. The ground clearance G was set to $G = 50$ mm for the Ahmed body and $G = 43$ mm for the C4 while a flap is mounted along the trailing edge of the raised floor to compensate for blockage. The free-stream velocity, monitored by a Pitot probe located at 2m from the grids, is $U_\infty = 20 \pm 0.2$ m/s, which corresponds to $Re_H = U_\infty H/\nu \approx 4 \times 10^5$, with ν the kinematic viscosity of air. The setup is shown in Figure 1. Free-stream turbulence is generated by regular bi-planar grids placed at the in-

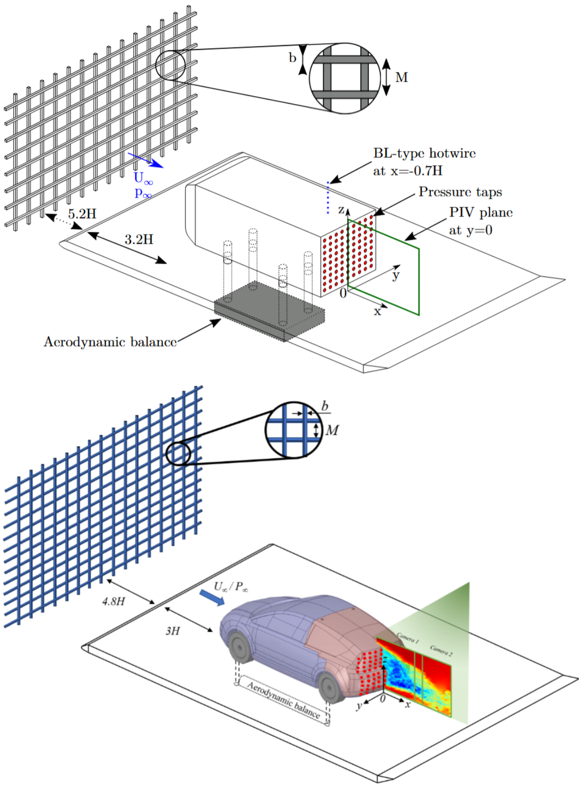

Figure 1. Schematic showing the two different models for the Ahmed body (top) and the Citroën C4 model (bottom) showing the location of measurements for the comparative study.

/	C_D	C_b	κC_p	$2\kappa\overline{u'^2}$	-$2\overline{u'w'}$	L_R	$\dot{m}_e$
Ahmed	0.33	0.27	98%	-28%	30%	1.57	0.093
C4	0.26	0.18	84%	-4%	20%	0.68	0.057

Table 1. Summary of the different contributions to the drag coefficient.

let of the test section (1.5 m upstream of the leading edge of the raised floor). In this study, three grids with square bars were considered, each of them being characterised by a solidity defined as $\chi = b/M(2-b/M) = [16,48,55]$ % where $M = [143,320,360]$ mm and $b = [25,90,120]$ mm stand for the grid mesh and the bar thickness (see figure 1), and produce turbulence intensities

$$Tu = \sqrt{\overline{u'^2}}/U_\infty \approx [4.8,9,13](\%), \tag{1}$$

respectively. These measurements were obtained using a hot wire located at the same longitudinal position than the back of the body but at the centre of the test section. Note that this position is also where the origin is set, as shown in figure 1. In addition, longitudinal profiles of turbulent intensity were performed in the test section in order to correct the measurements obtained from the Pitot tube. The grid and free-stream turbulence properties are summarised in Passaggia *et al.* (2021).

3 Methodology

The equations for the conservation of mass and momentum are made non-dimensional using U_∞ as the velocity scale and the height of the body H as a lengthscale. The non-dimensional quantity therefore reads

$$x_i = x_i^*/H, \quad u_i = u_i^*/U_\infty, \quad p = p^*/\rho U_\infty^2.$$

Flow solutions are then split between a temporal mean U and a fluctuation u' using Reynolds' decomposition

$$u_i(x_i,t) = U(x_i) + u'(x_i,t), \quad p(x_i,t) = P(x_i) + p'(x_i,t).$$

The total drag coefficient hence writes

$$C_D = \frac{2F_D}{\rho HWU_\infty^2}, \tag{2}$$

where W is the width of the body. Note that the aspect ratio $H/W = 0.84$ for the Ahmed body and 0.8 for the C4 model. The base-pressure drag is obtained as

$$C_b = \frac{1}{HW}\iint_S C_p(y,z)\,\mathrm{d}S, \tag{3}$$

integrated over the base of each body, where $C_p = 2(P - P_\infty)/\rho U_\infty^2$ and where P_∞ is the static pressure far from the body. Further, the contributions to the base-pressure drag are analysed by means of a momentum budget evaluated along the recirculation region connects the base to the near wake. In order to determine the contours of the recirculation region, thereby defining a closed control volume for the analysis, we use the Recirculation Region Interface (Stella *et al.*, 2017*b*) defined as

$$RRI = x_i\Big|_{U=0}. \tag{4}$$

Using the vertical mid plane, located at the centre of the vehicles (i.e. $y = 0$), the momentum budget simplifies to

$$C_b \sim \int_G^h C_p(x=y=0,z)\,\mathrm{d}z = \int_{RRI} [\kappa(C_p + 2\overline{u'^2}) - 2\overline{u'w'}]\mathrm{d}x, \tag{5}$$

where $\kappa = \mathrm{d}z/\mathrm{d}x$ and $h \leq H$ is the height at which the RRI reconnects to the base of the body (see figure 2 for the details on each wake). In this configuration, the static pressure in the test section is not uniform and compensates the local turbulence level T_u^2. In order to circumvent this problem, the static pressure $p_\infty(x)$ was corrected using hot-wire measurements performed in the free-stream at different streamwise locations, allowing for correcting the static pressure obtained at the rear of the bluff bodies as well as the free-stream velocity as measured by the Pitot tube (Bailey *et al.*, 2013).

In addition to the momentum budget, the mass-entrained across the RRI defines the mean amount of fluid entrained inside the near wake and writes

$$\dot{m}_e = \rho \int_{RRI} W_{in}\,\mathrm{d}x. \tag{6}$$

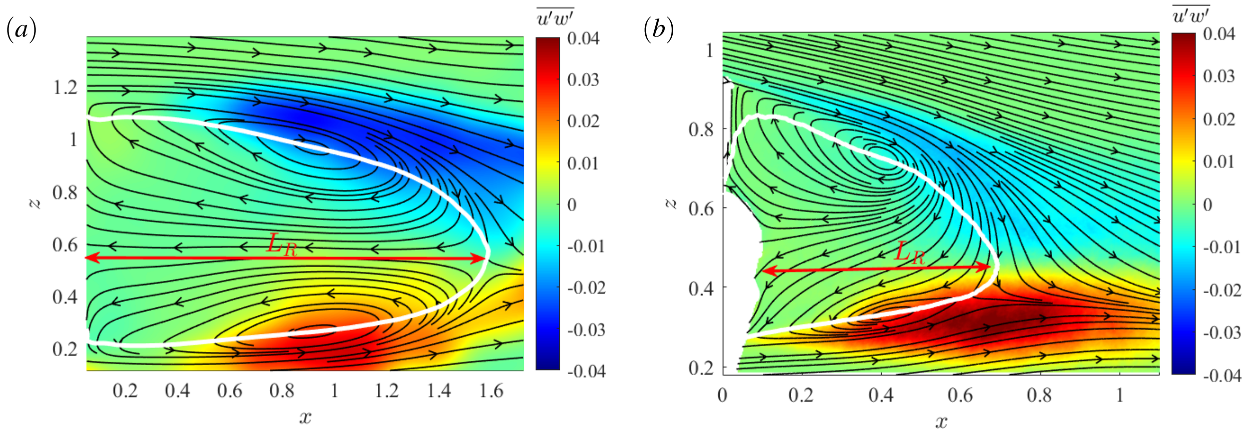

Figure 2. Schematic of the two wakes for (a) the Ahmed body and (b) the Citroën C4 model measured in the mid-plane at $y = 0$ where streamlines in black are overlapped onto the recirculation region interface (shown in white) where mass and momentum budgets are calculated. The length of the recirculation region is also shown in red.

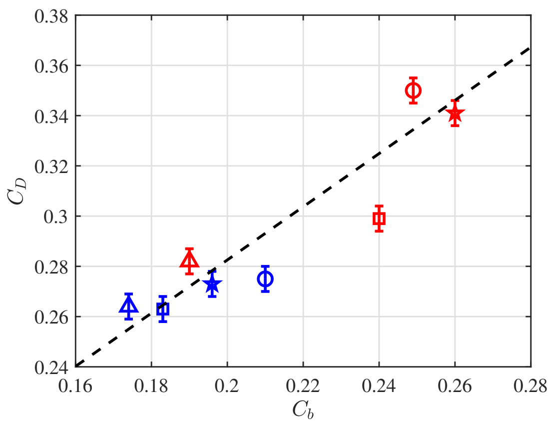

Figure 3. C_D as a function of C_b for (red) the Ahmed body and (blue) the C4 model and for the three turbulence grids that is $T_u \approx 0.4\%\,(\star)$, $T_u \approx 4.8\%\,(\circ)$, $T_u \approx 9\%\,(\square)$, $T_u \approx 13\%\,(\Delta)$. The dashed line shows the fit $C_D = C_b + 0.08$.

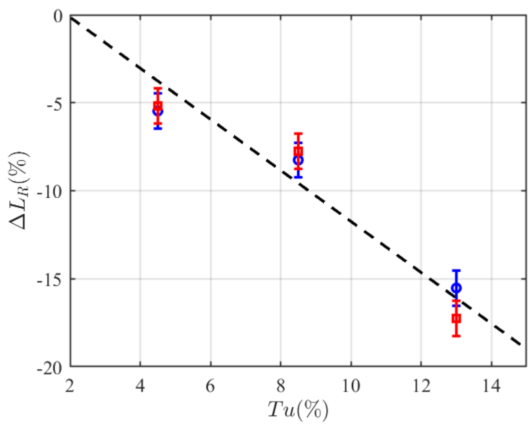

Figure 4. Recirculation length variations in (%) of ΔL_R as a function of the turbulence intensity Tu for (red) the Ahmed body and (blue) the C4 model.

where W_{in} is the vertical component of the velocity entering the recirculation region. Moreover, there exists a link between the mass and the momentum budget. As shown in Stella *et al.* (2018), the mean pressure can be partially linked to the mass entrained through the use of the circulation and Kelvin's theorem. In other words, the mass entrained can be used as a proxy in order to evaluate how the pressure from the mean flow affects the pressure at the base.

4 Drag to base-pressure analysis

Force measurements are reported in figure 3 for the different turbulence grids and for the two models considered in this study. It is worth noting that, in the case of both bodies, base-pressure modifications are directly proportional to the drag coefficient, meaning that base-pressure drag essentially drives the total drag. Furthermore, the ratio of base- to total-drag is close to 0.82 for the Ahmed body and 0.69 for the C4 model, which is relatively close. In addition, as shown in figure 3, variations of the base-to-total-drag coefficient remains linear throughout the entire set of experiments, that is $C_D \sim C_b$ which hints at a common mechanism acting on the wake of these bluff bodies.

5 Mass-entrainment and RRI analysis

Analysing the length of the recirculation region, both cases show that L_R decreases linearly with increasing turbulence intensities, as shown in figure 4 while the base pressure drag both increases or decreases depending on the value of Tu, which is odd with the current understanding of bluff-body near wakes in the presence of turbulence.

In order to provide a comparative analysis, all quantities are normalised using the reference case, such that

$$\Delta L_R = (L_R - L_{R,0})/L_{R,0}. \quad (7)$$

where $L_{R,0}$ is the recirculation length measured for the reference case when $Tu \approx 0$ (all reference values are reported in table 1). Using this approach, both bodies now show the same evolution for this normalised recirculation length, meaning that the lengthscale of reference remains the recirculation length, independently of the geometry.

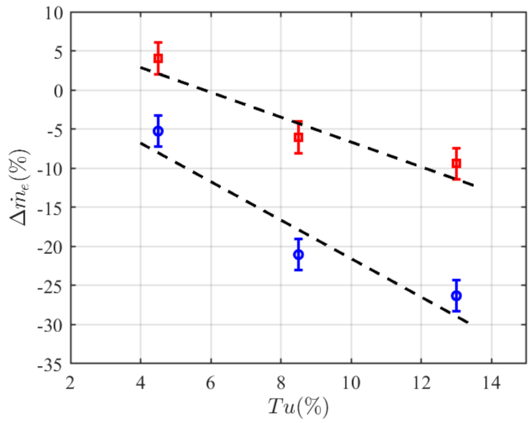

Figure 5. Evolution of the mean mass entrained $\Delta\dot{m}_e$ (%) across the RRI in the vertical plane as a function of the turbulence intensity Tu for (red) the Ahmed body and (blue) the C4 model.

The mass entrained into the wake is reported in figure 5 where the mass entrained into the wake is also normalised and writes $\Delta\dot{m}_e = (\dot{m}_e - \dot{m}_{e,0})/\dot{m}_{e,0}$, where $\dot{m}_{e,0}$ is the mass entrained without free-stream turbulence. Similar to the observations for the recirculation length, the mass entrained into the wake decreases essentially linearly for both cases with respect to the turbulence intensity. In fact, there is a direct link between both quantities since they are both linearly dependent on Tu, which provides

$$\Delta\dot{m}_e \sim \Delta L_R,$$

and therefore hints to the idea that the entrainment velocity remains essentially constant and that the recirculation length is the main control parameter for mass entrainment, independently of the geometry of the body.

6 Momentum budget analysis

Contributions to the base drag are directly linked to the momentum budget integrated along the recirculation-region interface in eq. (5) where each term was measured or estimated using particle image velocimetry and a pressure scanner for both cases and for all turbulence grids (see figure 4(a,b) for the details of the wake structure and the Reynolds shear stress). The approach to obtain pressure is detailed in Shanmughan *et al.* (2020); Passaggia *et al.* (2021). Similar to the analysis for the mass entrained in the near wake, we report the normalised evolution for each term evaluated along the RRI. Since pressure is the dominant term, as reported in table 1, we report its dependence in figure 6 where both geometries display very different behaviours and signs. In the case of the Ahmed body, and similar to the results obtained in Passaggia *et al.* (2021); Zeidan *et al.* (2023) along the separatrix, the contribution of the pressure to the base drag decreases by 40% between the lower and the larger value of the turbulence intensity. In contrast, the contribution of the pressure term for the realistic car model remains essentially unaffected by free-stream turbulence. Its contribution increases by 17% when adding free-stream turbulence (which is actually linked to the earlier transition of the boundary layer developing along the raised floor).

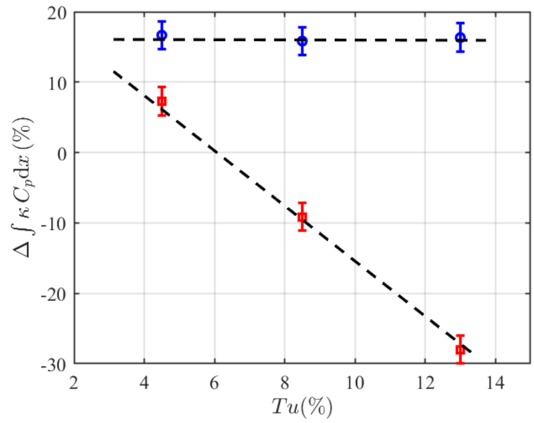

Figure 6. Difference of contribution in (%) of the pressure term in the momentum budget along the RRI as a function of the turbulence intensity Tu for (red) the Ahmed body and (blue) the C4 model.

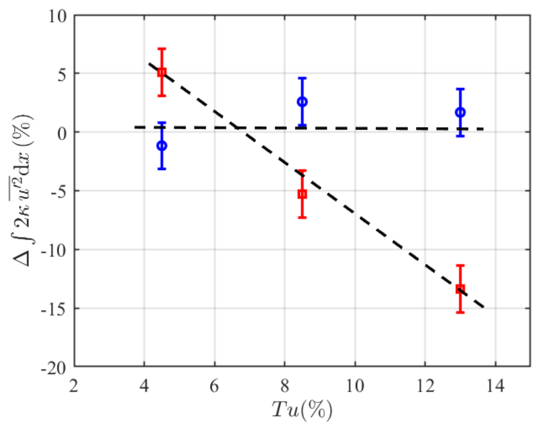

Figure 7. Difference of contribution in (%) of the turbulent normal stress term in the momentum budget along the RRI as a function of the turbulence intensity Tu for (red) the Ahmed body and (blue) the C4 model.

Although pressure is the dominant term for the case of the Ahmed body, turbulence plays up to a third of the contribution at the base of the Ahmed body and 20% for the C4 model (see table 1). This quantity is further investigated, in order to understand the response of the flow to free-stream turbulence. The effect of free-stream turbulence on the contribution of the normal stresses is shown in 7. The results obtained on the RRI provide the same results that were obtained on the separatrix in Passaggia *et al.* (2021) on the Ahmed body and decrease linearly by 20% with increasing free-stream turbulence intensity. This is again at odds with the results obtained on the realistic car model where the contribution of the normal stresses remains, once again, essentially independent of the free-stream turbulence intensity.

As a result, the base-pressure drag of the realistic car model is only dictated through the evolution of the Reynolds stresses to the momentum budget. Their evolution is reported in figure 8 for both geometries and shows once again very similar behaviour with respect to the Ahmed body. For both cases, the contribution of the Reynolds shear stress to the momentum budget decreases by 12 % for both geometries. As shown in Passaggia *et al.* (2021) the mechanisms associated with the de-

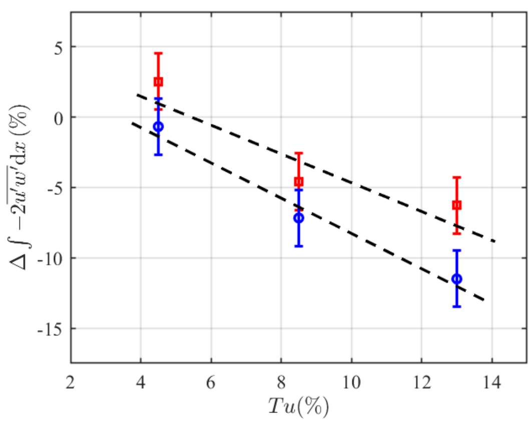

Figure 8. Difference of contribution in (%) of the turbulent shear stress term in the momentum budget along the RRI as a function of the turbulence intensity *Tu* for (red) the Ahmed body and (blue) the C4 model.

crease of the Reynolds stresses and therefore the variations of drag are quite different for both geometries. On one hand, the Ahmed body shows a reduction of the Kelvin-Helmholtz instabilities on the upper and lower shear layers (see Passaggia *et al.* (2021) for a complete analysis). On the other hand, the wake in the C4 displays a different mechanisms which is associated with turbulent diffusion term which is characterized by rare but violent events near the end of the recirculation region, and associated with the "breathing of the recirculation region", which is also present in the case of the Ahmed body but overshadowed by the reflectional symmetry breaking of the wake (Volpe *et al.*, 2015). This aspect will be analysed in more details during the presentation.

7 Conclusion

While the Ahmed body is often used as a surrogate for analysing the effect of flow-control devices (Grandemange *et al.*, 2013*b*; McNally *et al.*, 2019) or the external factors such as side winds (Bonnavion *et al.*, 2017) or free-stream turbulence (Passaggia *et al.*, 2021) on road vehicles, this study shows a more nuanced reality. For instance, only considering integral quantities such as the total drag or the base-pressure drag on local quantities such as the recirculation region or mass entrainment alone might provide illusive conclusions. For instance, in the case of the Citroën C4 coupé model, and despite normalized characteristics, free-stream turbulence has a dramatic effect on the Ahmed body while the realistic car model is four times less receptive. Furthermore, the drag budget for the realistic car model is essentially controlled by the Reynolds shear stress term, along the lower shear layer, associated with the lower recirculation region interface. This clearly hints to the idea that control strategies for a realistic car geometries will be less efficient than for an Ahmed body. This was recently shown in Abed-Meraim *et al.* (2025) for the same car model; While Grandemange *et al.* (2013*b*) showed very promising effects of flaps to improve the aerodynamic drag of an Ahmed body, results reported for a realistic car geometry show a very different sensitivity Abed-Meraim *et al.* and are further aligned with the results obtained for a full-size vehicle, as reported in Sebben *et al.* (2017). This study therefore calls for a warning when attempting to transpose control strategies from canonical bluff bodies to realistic geometries.

Acknowledgement The authors acknowledge the contribution of Stéphane Loyer, research engineer at PRISME laboratory, for is contribution in setting up the experiment and his assistance during data collection.

REFERENCES

Abed-Meraim, A., Passaggia, P.-Y. & Kourta, A. 2025 Caractérisation et contrôle du sillage proche d'un véhicule réel. In *26e Congrès Français de Mécanique*.

Ahmed, S. R., Ramm, G. & Faltin, G. 1984 Some salient features of the time-averaged ground vehicle wake. *SAE Trans.* pp. 473–503.

Bailey, S. C. C. *et al.* 2013 Obtaining accurate mean velocity measurements in high reynolds number turbulent boundary layers using pitot tubes. *J. Fluid Mech.* **715**, 642–670.

Bonnavion, G. 2018 Dynamics of the unstable wake modes in automotive aerodynamics: from simplified models to real vehicles. Phd thesis, Université Paris-Saclay.

Bonnavion, G., Cadot, O., Évrard, A., Herbert, V., Parpais, S., Vigneron, R. & Délery, J. 2017 On multistabilities of real car's wake. *J. Wind Eng. Ind. Aerodynamics* **164**, 22–33.

Grandemange, M., Gohlke, M. & Cadot, O. 2013*a* Turbulent wake past a three-dimensional blunt body. Part 1. Global modes and bi-stability. *J. Fluid Mech.* **722**, 51–84.

Grandemange, M., Mary, A., Gohlke, M. & Cadot, O. 2013*b* Effect on drag of the flow orientation at the base separation of a simplified blunt road vehicle. *Exp. Fluids* **54** (5), 1529.

Khan, T. I., Pastur, L., Cadot, O. & Parezanović, V. 2024 Equilibrium of fluid fluxes in the wake of a three-dimensional flat-back bluff body. *J. Fluid Mech.* **997**, A60.

McNally, J., Mazellier, N., Alvi, F. & Kourta, A. 2019 Control of salient flow features in the wake of a 25^o ahmed model using microjets. *Exp. Fluids* **60** (1), 7.

Passaggia, P.-Y., Mazellier, N. & Kourta, A. 2021 Aerodynamic drag modification induced by free-stream turbulence effects on a simplified road vehicle. *Phys. Fluids* **33** (10), 105108.

Sebben, S., Sterken, L. & Wölken, T. 2017 Characterization of the rear wake of a suv with extensions and without extensions. *Proceedings of the Institution of Mechanical Engineers, Part D: Journal of Automobile Engineering* **231** (9), 1294–1302.

Shanmughan, R., Passaggia, P.-Y., Mazellier, N. & Kourta, A. 2020 Optimal pressure reconstruction based on planar particle image velocimetry and sparse sensor measurements. *Exp. Fluids* **61** (11), 1–19.

Stella, F., Mazellier, N., Joseph, P. & Kourta, A. 2018 Mass entrainment-based model for separating flows. *Physical Review Fluids* **3** (11), 114702.

Stella, F., Mazellier, N. & Kourta, A. 2017*a* Scaling of separated shear layers: an investigation of mass entrainment. *J. Fluid Mech.* **826**, 851–887.

Stella, F., Mazellier, N. & Kourta, A. 2017*b* Scaling of separated shear layers: an investigation of mass entrainment. *J. Fluid Mech.* **826**, 851–887.

Volpe, R., Devinant, P. & Kourta, A. 2015 Experimental characterization of the unsteady natural wake of the full-scale square back Ahmed body: flow bi-stability and spectral analysis. *Exp. Fluids* **56** (5).

Zeidan, W., Mazellier, N., Guilmineau, E., Passaggia, P.-Y. & Kourta, A/ 2023 A near-wake survey of an ahmed body comparing low-& high-fidelity numerical models with experiments. *Euro. J. Mech.-B/Fluids* **101**, 195–208.